SUMMARY OF WORKING GROUP ON WEAK-STRONG BEAM-BEAM EFFECTS

E. Keil, CERN, Geneva, Switzerland

Abstract

This paper summarizes the presentations and discussions in the working group on weak-strong beam-beam effects at the LHC Beam-Beam Workshop, held at CERN on 12 to 16 April 1999. It also gives answers to questions that had been raised by the organizing committee prior to the workshop.

1 INTRODUCTION

This paper summarizes the presentations and discussions in the working group on weak-strong beam-beam effects at the LHC Beam-Beam Workshop, held at CERN on 12 to 16 April 1999. The discussions were organized around the following topics: Measurable quantities and instrumentation, experiments, and simulation. This summary also gives answers to questions that had been raised by the organizing committee prior to the workshop, both general questions to both working groups, and specific questions to the working group on weak-strong beam-beam effects.

2 CONTRIBUTED TALKS ON WEAK-STRONG EFFECTS

The working group heard the talks listed below and discussed them to various degrees. The labels in bold letter are those appearing in the workshop programme. The written versions of these talks will be in these proceedings. The results will be discussed in the appropriate section(s) below.

CWS4 Influence of Vertical Dispersion and Crossing Angle on the Performance of the LHC, L. Leunissen

CWS1 Incoherent beam-beam tune shifts in the LHC, H. Grote

CWS5 Effect of the beam-beam interactions on the dynamic aperture and amplitude growth in the LHC, T. Sen

CWS6 Weak-strong beam-beam simulations for the LHC, F. Zimmermann

CWS2 Filling Schemes, Collision Schedules and Beam-beam Equivalence Classes, J. Jowett

CWS3 Application of Beam-beam Interaction to a Particle Density Function, T. Koyama

CWS7 Effect of Very Low Frequency Ground Motion on the LHC, L. Vos

3 MEASURABLE QUANTITIES AND INSTRUMENTATION

The working group started the discussion of measurable quantities and instrumentation from P. Bagley's list of Tevatron instrumentation. The consensus reached at the end of the discussion is summarized below.

In order to measure the *beam lifetime* a current transformer DCCT is needed that accurately measures the total beam currents. A fast bunch integrator and a sampled bunch display for the bunch currents are also needed in order to quickly identify bunches with shorter than average lifetimes.

In order to measure bunch parameters at the interaction points, e.g. the *rms beam radii* σ^*, the *offsets* Δx^* and Δy^*, and the *luminosity* L, a combination of beam-beam luminosity scans, beam-beam deflection scans, beam-beam transfer function measurements, luminosity and vertex detectors are needed.

In order to measure the *tunes* $Q(J)$ as functions of the actions J, to obtain *footprints* and *tune modulation*, AC dipoles operating close to the fractional parts of Q will be used in RHIC, and a resonant Schottky cavity has been used in the Tevatron. A bunch-by-bunch feedback system can also be used to excite bunches, and measure their response. and stepped kicker magnet in LHC, bunch-by-bunch tunes by gated beam excitation and response

Movable collimators can be used to measure density distributions in the tails and diffusion rates.

The rms emittance growth and hence its growth in time can be measured with flying wires, that cause a small emittance growth on each traversal, and less destructively by ion profile and synchrotron light monitors.

F. Willeke emphasizes the usefulness of loss monitors for checking the health of HERA.

The working group did not know whether the LHC will have a bunch-by-bunch feedback system that can also be used to excite bunches, and systems for measuring tails.

4 EXPERIMENTS

S. Peggs had advocated organized experiments that are proposed to and approved by Program Committees at existing colliders like particle physics experiments as one way of getting experimental answers to questions, quoting the E778[1] experiment as an example. Such experiments require (i) a model, applied to a configuration in a specific machine, making predictions for measurable quantities, (ii) verifications that machine behaves according to the model, and (iii) confronting model and experiment. S. Peggs also mentioned that RHIC can be filled quickly and offers possibilities for formal experiments on crossing angle, head-on and/or parasitic collisions, some immediately, some others later on after upgrades. However, watching the commissioning of RHIC and Tevatron Run II might be the best method for accumulating information relevant to LHC.

5 SIMULATION

The participants from FNAL use MAD, SIXTRACK, TEVLAT and Sen's unnamed code for Tevatron and LHC work. The participants from CERN use BBC, MAD, SIXTRACK and Zimmermann's code. Codes mentioned in passing were Shatilov's code LIFETRAC, and similar codes by Irwin and Siemann et al.

The participants agreed that codes should be validated by comparing their results on observable quantities with those of other codes, experiments, and analytical results. The teams of experimenters, confronting the codes with reality, should preferably be different from the teams of code developers. We are not too optimistic about getting analytical results for complicated cases. Hence, the validity of codes is at best demonstrated in a restricted range of parameters. Code validation is also necessary to make users feel confident about the results of codes other than their own.

There is no shortage of beam-beam simulation codes. Complicated code(s) with (most of) the physics are needed to get close to reality. However, we fear that it/they are slow, and therefore cannot be used for extensive parameter searches. Hence, we also need less complicated, faster codes, including only the most important physics, selected by judgement/prejudices of the developer(s), to quickly eliminate parameter ranges that don't work.

All simulation codes consist of a module that reads a machine description, a small number of modules that track particles through the machine, and generate large unreadable tracking tables, and modules that display the results to the user. Different codes should get identical machine descriptions, cf. the SXF effort[2] for LHC descriptions, understood by MAD, SIXTRACK, TEAPOT, TEVLAT, and possibly other programs. Further development of tracking codes would be easier with a library of well-documented modules, e.g. for 4D or 6D beam-beam kicks, maps through non-linear elements and/or entire arcs, etc. WWW is one way of providing access to modules. Note that tracking invokes only a small number of modules, selected by judgement and/or prejudices of the developer(s) of what physical effects are important. The comparison of results would be facilitated by adopting common styles of inspection and presentation.

6 GENERAL QUESTIONS

The working group took the liberty of reformulating some of the general questions raised with both working groups before trying to answer them. The questions are printed in roman, the answers are printed in *italics*.

Do you know a reason why the present choice of the LHC working point (64.31, 59.32) might be bad?
Working points (64.232, 53.242) and (64.385, 53.395) are crossed by fewer non-linear resonances.

How are the beams brought into collision in existing and planned colliders?
The Tevatron beams were brought into collision by longitudinal cogging in the past. This will no longer be possible in Run II. Hence, the beams will be brought into collision transversely within a few seconds, given by the discharge time of the electrostatic separators. In HERA the beams are brought into collision transversely at slow speed. In RHIC the beams are injected and accelerated with the RF frequencies of the two rings unlocked, and then brought into collision longitudinally and transversely. The question was raised whether overlap knockout resonances that were observed in the ISR[3], might occur while the two beams are unlocked.

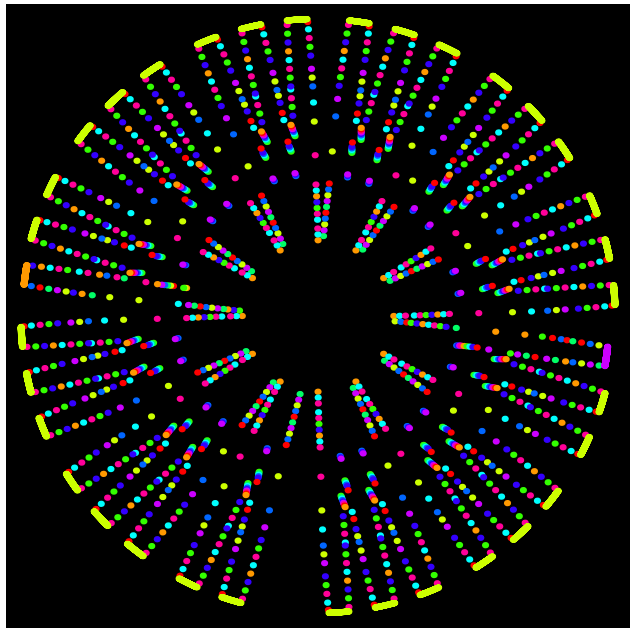

Figure 1: Equivalence classes for nominal LHC. Bunches in a given beam-beam equivalence class are represented here as points of identical colour on a circle of a given radius. Note details! This example was computed ignoring parasitic encounters around IP2 and IP8 (cf. J. Gareyte's talk), so reducing the number of classes from 176 to 152.

Do you know a reason why the same procedures do not work for LHC? *No*

Do we expect luminosity or beam lifetime degradation from ground motion, dynamic effects (e.g. tune ripple) and chromaticity?
According to model of L. Vos, the two beams will get separated as in a random walk, unless they are kept centered every so many minutes. Although the model was questioned, the conclusion is most likely correct. It should be checked with standard ATL models. Tune modulation with $\Delta Q \approx 10^{-4}$ *at* Q_s *had no effect in Zimmermann's simulation;* $Q' \leq 5 \ldots 6$ *with* $\sigma_e \approx 4 \cdot 10^{-4}$ *works in Tevatron. To avoid drop in luminosity lifetime in SPS* $\Delta Q \leq 2 \cdot 10^{-4}$.

What procedures shall be followed to validate beam-beam design choices?
Answers in section on simulation and experiments.

What are the implications of beam-beam effects for linear optics, machine instrumentation and operation?

Keeping track of more than 4000 bunches with only about half of them in the most populated equivalence class, as discussed by J. Jowett, and producing meaningful displays for the operators is a tough job for the controls people, and should be tackled soon. Fig. 1 shows an example of equivalence classes.

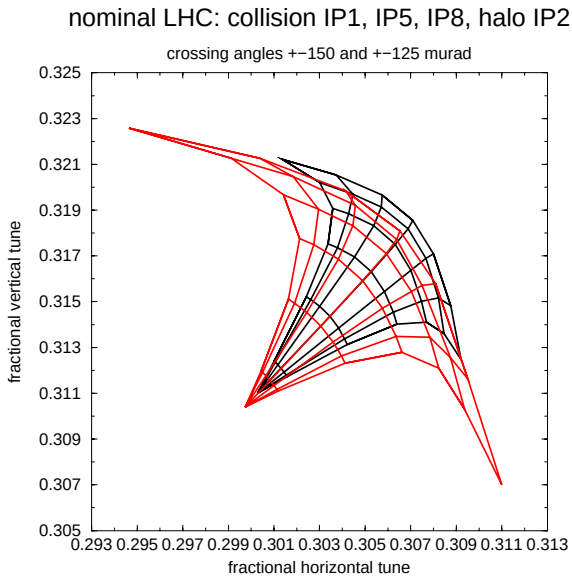

Figure 2: Footprints for nominal LHC with head-on collisions in IP1, IP5 and IP8, and halo collisions in IP2, for half crossing angles ± 125 μr in red and ± 150 μr in black.

7 CONSEQUENCES OF THE INSERTION TRIPLET ERRORS

The first question for the working group on weak-strong effects was: Given the triplet errors, can we recommend an optimum crossing angle? We deal with the rather lengthy answer in this section. The quadrupole triplets for the interaction points 1 and 5 come from FNAL and KEK. Their systematic and random field errors are different[4]. The quadrupoles from one source can be installed near one interaction point each, or they can be mixed. Computations of the footprints were presented by H. Grote. Tab. 1 shows a comparison of the standard ingredients. The number of long-range collisions is inconsistent.

Fig. 2 shows the extra contribution of the parasitic collisions in the NW-SE direction to the footprint when the half crossing angle is reduced from 150 to 125 μr. Fig. 3 shows the increase of the footprint when the field error b_{10} is added. Fig. 4 shows the change of the footprint when the head-on collision at IP1 is removed, simulating a super-pacman bunch. The size in the SW-NE direction shrinks. All footprints were calculated at injection tunes, and then moved because of the tune-finding procedure.

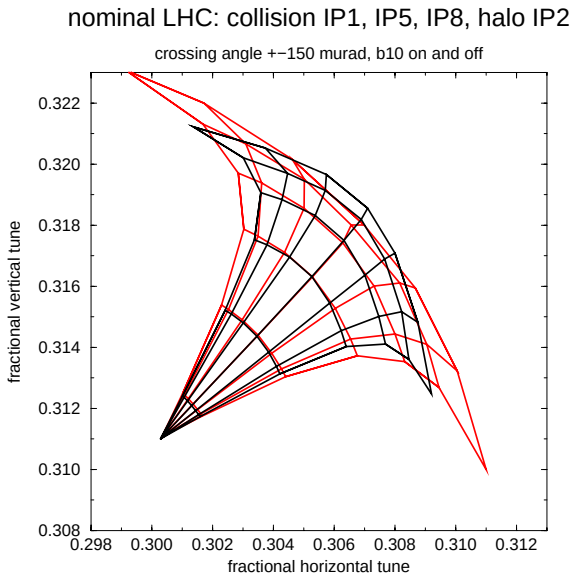

Figure 3: Footprints for nominal LHC with head-on collisions in IP1, IP5 and IP8, and halo collisions in IP2, for a half crossing angle ± 150 μr with b_{10} triplet errors in red and without in black.

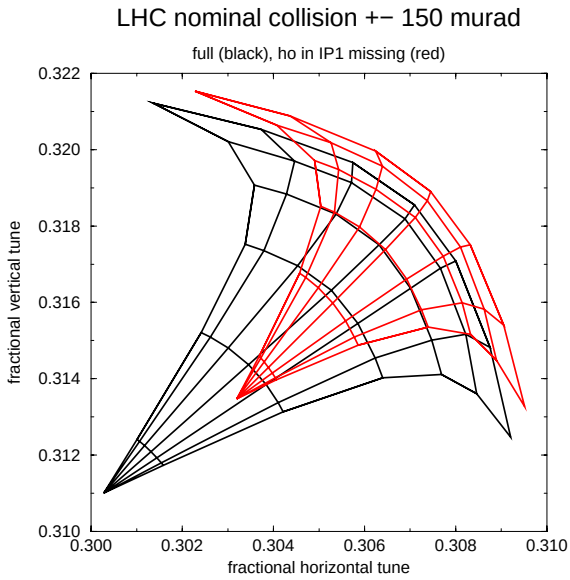

Figure 4: Footprints for nominal LHC with head-on collisions in IP5 and IP8, and halo collisions in IP2, for a half crossing angle ± 150 μr, and with head-on collisions in IP1 in black and without in red.

7.1 Grote's Tracking Results

An argument arose during the workshop about the validity of tracking results for rather small numbers of turns.

Table 1: Ingredients of simulations. The values of kicks/quadrupole apply to the interaction region triplet. Element misalignments and compensation of triplet nonlinearities are not included. Values shown are the standard choices. Other choices are explicitly stated in text and figures. Abbreviations: H-H head-on collisions with horizontal crossing angle, H-V head-on collisions with vertical crossing angle, Ha-V halo collisions with vertical crossing angle, L long-range parasitic collisions, LL lumped long-range parasitic collisions, N/A not applicable.

Author	Grote	Leunissen	Schmidt	Sen	Sen	Zimmermann
Program	MAD	BBC	SIXTRACK	TEVLAT		
LHC	5	5	5	5.1	5.1	5
Dimensions	6	6	6	6	6	4
Turns	$5\ 10^4$	10^4	10^5	10^5	10^5	10^3
Arc nonlin.	Sext	No	Sext	Sext	No	No
Kicks/Quad	IP1+5:4, IP2+8:2	1	IP1+5:4, IP2+8:2	$1-3$	N/A	1
Syst. errors	[4]	No	[4]	[4]	No	[4]
Rand. errors	No	No	No	Yes	No	Yes
Beam-Beam	Yes	Yes	No	Yes	Yes	Yes
Slices	H:5, L:1	5		1	H:5, L:1	1
IP1	H-V+28L	H-V		H-V+30L	H-V+30L	H-V+36LL
IP2	Ha-V+28L					
IP5	H-H+28L			H-H+30L	H-H+30L	H-H+36LL
IP8	H-V+28L					
X angle	$\pm 150\mu$r	$\pm 100\mu$r		$\pm 150\mu$r	$\pm 150\mu$r	$\pm 150\mu$r

H. Grote quickly computed the results shown in Fig. 5. There was no observable emittance growth.

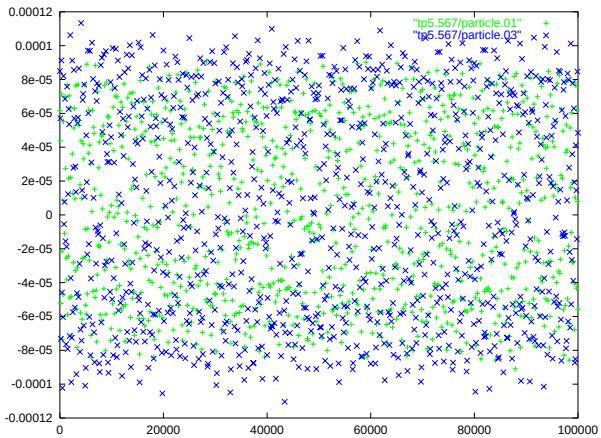

Figure 5: H. Grote's tracking results for collisions at ± 150 μr, all 4D beam-beam elements present, full error table for triplet quadrupoles including systematic and random, KEK at IP1 and IP8, FNAL at IP2 and IP5, tracking one particle at 5σ in green and 7σ each in blue, $\Phi = 45°$, $\Delta p = 2\sigma$ over 10^5 turns. The ordinate is the vertical particle coordinate y at IP1 in m, where $\sigma \approx 16$ μm.

7.2 *Schmidt's Tracking Results*

The simulation results of F. Schmidt in Fig. 6 demonstrate that the field errors cause a limitation of the dynamic aperture, even in the absence of beam-beam collisions, and serve as a yardstick for simulation results including beam-beam effects. The systematic error per arc is added to the mean values such that the absolute value of the error increases. The errors at the ends of the triplet quadrupoles are included.

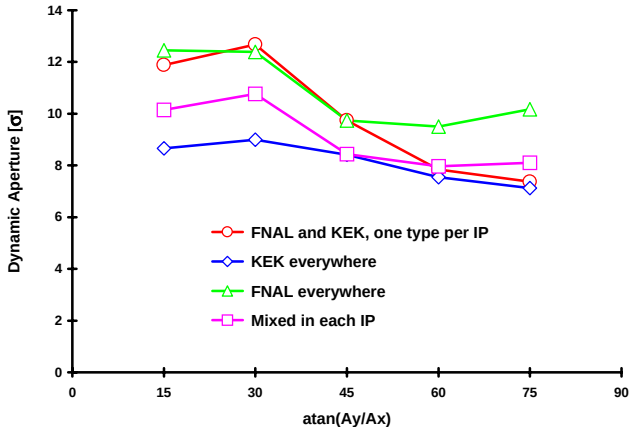

Figure 6: F. Schmidt's 6D tracking results for the dynamic aperture as functions of $\arctan(A_x/A_y)$ without beam-beam effects. The amplitudes A_x and A_y are scanned from 6 to 12 σ in steps of $\sigma/30$. The initial momentum error corresponds to 75% of the half bucket height.

7.3 *Sen's Tracking Results*

Fig. 7 shows Sen's result for the dynamic aperture as a function of the full crossing angle. Particles were launched

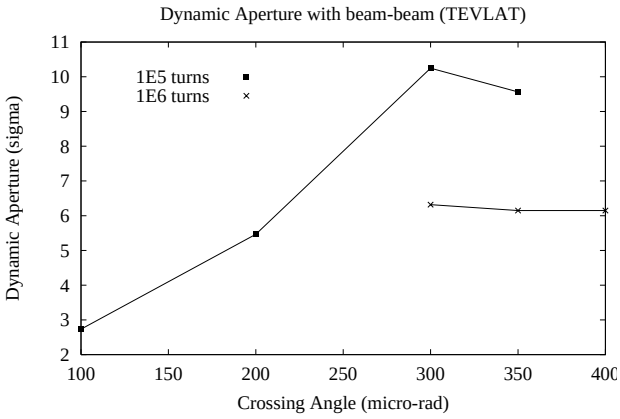

Figure 7: Dynamic aperture as a function of crossing angle. Single particles (on momentum) are tracked along the diagonal in emittance space with beam-beam and triplet errors[4] for 10^5 and 10^6 turns using TEVLAT. The quadrupoles are mixed, cf. Tab. 2.

along the diagonal in emittance space. For 10^5 turns tracking, the crossing angle was varied between 100 and 350 μrad and one seed was used for the random errors. For 10^6 turns tracking, the crossing angle was varied between 300 and 400 μrad and two random seeds were used. This longer term tracking shows that the dynamic aperture is relatively flat at around 6 σ in the range between 300 and 400 μrad. There is a maximum at 300 μr. The dynamic aperture at lower crossing angles is comparable to the separation between the beams (in units of σ) in the drift region. The dynamic aperture does not fall as steeply when the crossing angle is increased beyond 300 μr.

Table 2: Sen's comparison of mean and standard deviation of the dynamic apertures DA for FNAL and KEK quadrupole triplet errors with and without beam-beam collisions BB for 10^3 turns. Mixed magnets is one where the Q1 and Q3 are KEK magnets and Q2a, Q2b are FNAL magnets at both IR1 and IR5.

Triplet Errors	BB	DA
FNAL in IR1 & IR5	Off	11.2 ± 1.7
KEK in IR1 & FNAL in IR5:		
KEK $\langle b_{10} \rangle$=-1.0	Off	9.0 ± 0.9
KEK $\langle b_{10} \rangle$=-0.25	Off	11.1 ± 1.1
Mixed magnets:		
KEK $\langle b_{10} \rangle$=-0.25	Off	11.7 ± 1.2
KEK $\langle b_{10} \rangle$=-0.25	On	11.0 ± 1.1

Tab. 2 shows T. Sen's results for the dynamic aperture with several quadrupole triplet errors and with and without beam-beam collisions from tracking for 10^3 turns. Mixing the magnets improves the dynamic aperture by about 0.6σ. The results without beam-beam collisions may be compared with those in Fig. 6 for 10^5 turns. Including beam-beam interactions reduces the aperture by 0.7σ with 1000 turn tracking. However, tracking for 10^5 and 10^6 turns shows that the beam-beam collisions decrease the aperture further by approximately 3σ. Without beam-beam collisions, the dynamic aperture typically decreases by about 1σ when going from 10^3 turns to 10^5 turns.

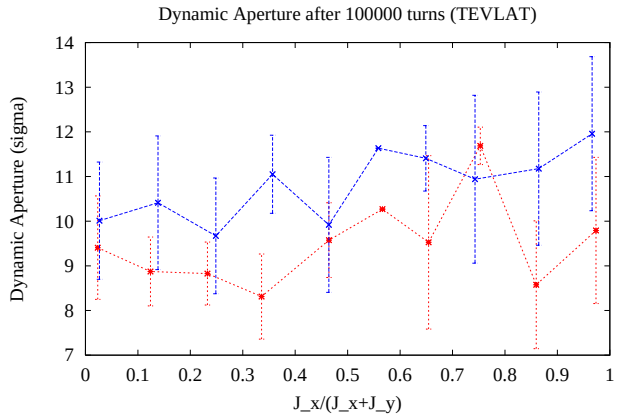

Figure 8: Dynamic aperture for particles tracked at 10 angles in emittance space (on momentum) for 10^5 turns without beam-beam interactions (blue) and with beam-beam interactions (read), and with triplet errors at a crossing angle of 300 μr. The quadrupoles are mixed, cf. Tab. 2. The data points and error bars represent the averages and the standard deviations over 5 seeds for the random errors[4] respectively.

Fig. 8 shows T. Sen's result for the dynamic aperture at 10 angles in emittance space, each averaged over 5 seeds, chosen from a Gaussian distribution. The dynamic aperture at this crossing angle and 10^5 turns is (10.8 ± 0.8) σ without beam-beam interactions and (9.5 ± 1.0) σ with beam-beam interactions. Comparing the dynamic aperture with and without the beam-beam interactions seed by seed for a proper statistical analysis shows that the average drop in dynamic aperture due to the beam-beam after 10^5 turns is (1.4 ± 0.4) σ. In some cases, systematic errors are included. The aperture is restricted at $\pm$30 mm in all IR quadrupoles and in the sextupoles in the arcs.

Sen's beam-beam code has the following features: (i) thin lens beam-beam kicks, including energy kicks a la Piwinski; (ii) exact treatment of the long-range kicks; (iii) the lattice is represented by a linear map; (iv) time-dependent tune and offset modulation and noise by an Ornstein-Uhlenbeck spectrum; (v) PACMAN bunches can be studied. Planned additions are approximations of the complex error function to speed up the code, and multipole fields in the triplets.

Figs. 9 and 10 show results from T. Sen's beam-beam simulation program in 4D and 6D simulations, respectively. In the 4D simulation, about 400 particles were distributed

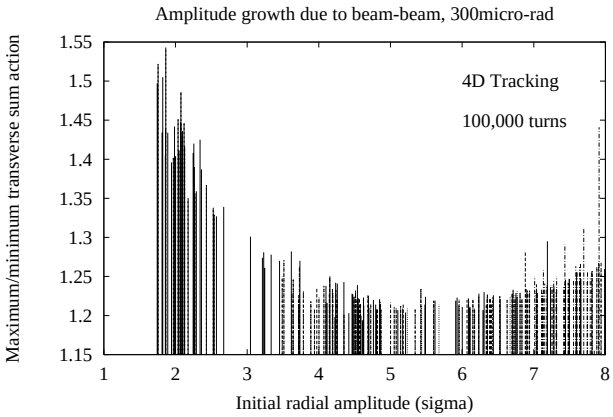

Figure 9: Tracking with T. Sen's beam-beam code with only head-on and long-range interactions at a crossing angle of 300 μr in 4D. The plot shows the relative amplitude growth as for initial radial amplitudes between 2 to 8 σ.

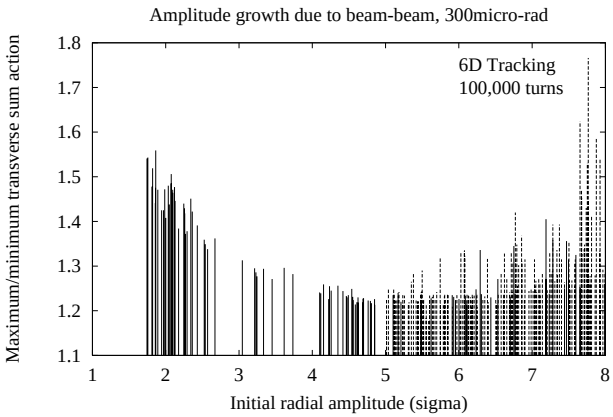

Figure 10: Tracking with T. Sen's beam-beam code with only head-on and long-range interactions at a crossing angle of 300 μr in 6D. The plot shows the relative amplitude growth for initial radial amplitudes between 2 to 8 σ.

with initial radial amplitudes ranging from 2 to 8 sigma and tracked for 10^5 turns, and the maximum relative amplitude growth is less than 1.55 for particles in the core between 2 and 3 σ, and about 1.3 for particles beyond 6 σ. This suggests that there may not be a problem with lifetime at this crossing angle. For the simulation in 6D, 250 particles were distributed with initial amplitudes ranging from 2 to 8 σ. Significant growth is now seen for particle amplitudes greater than 7.5 σ when synchrotron oscillations and energy kicks due to the beam-beam interaction are included.

Fig. 11 shows the maximum relative amplitude growth on a logarithmic scale as a function of the full crossing angle, obtained by T. Sen with his beam-beam simulation program. The relative amplitude growth below a crossing angle of 300 μr is very large, reaches about 450 at 100 μr,

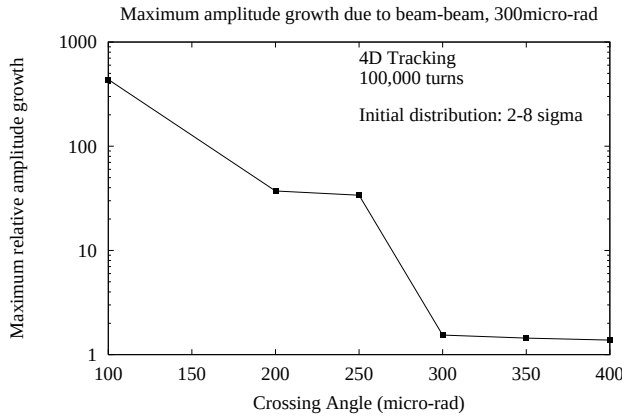

Figure 11: Maximum relative amplitude growth over all particles in the distribution at various crossing angles. Tracking done with T. Sen's beam-beam code for 10^5 turns. The ordinate is plotted on a log scale.

and suggests that the lifetime would be very low. At crossing angles of 300 μr and beyond, relative amplitude growth of particles in the 2 to 8 σ range does not exceed 1.3. This figure is somewhat similar to Fig. 17.

7.4 Zimmermann's Tracking Results

F. Zimmermann presented simulation results from his beam-beam simulation program which has the following ingredients: (i) Tune modulation in the linear arcs at the synchrotron tune Q_s takes care of chromaticity and synchrotron oscillations in an approximate manner. (ii) Five kicks are applied near each IP: Systematic and random triplet nonlinearities, parasitic collisions of round beams, lumped into a single kick, head-on collisions of round beams at a crossing angle, parasitic collisions of round beams, lumped into a single kick, systematic and random triplet nonlinearities.

Figs. 12 to 18 show a selection of Zimmermann's results. In particular, Figs. 12 and 13 show a comparison of the footprints without and with the FNAL field errors, demonstrating that the field errors indeed have an effect.

Figs. 14 and 15 show a comparison of the tune diffusion rates without and with the FNAL field errors, demonstrating that the field errors indeed have an effect. Zimmermann obtains the tune diffusion rate by measuring the tunes for the first and last batch of 500 turns, and displays the difference as a function of the initial amplitudes in x and y, measured in units of σ_x and σ_y.

Fig. 16 shows the action diffusion rate as a function of the initial amplitudes in x and y, measured in units of σ_x and σ_y at ± 150 μr half crossing angle for several arrangements described in the figure. A steep rise of the diffusion rate happens just below $6\sigma_{x,y}$ with head-on and long-range beam-beam collisions. Other simulations have shown that it is caused by the long-range beam-beam collisions. With-

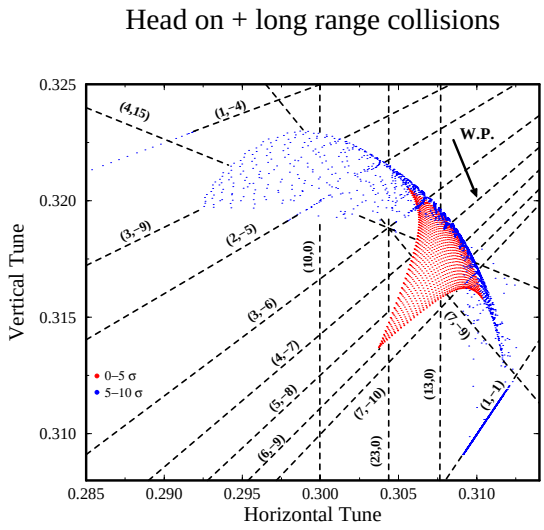

Figure 12: Zimmermann's results for the footprints without field errors. Red: $0 \ldots 5\sigma$, blue: $6 \ldots 10\sigma$

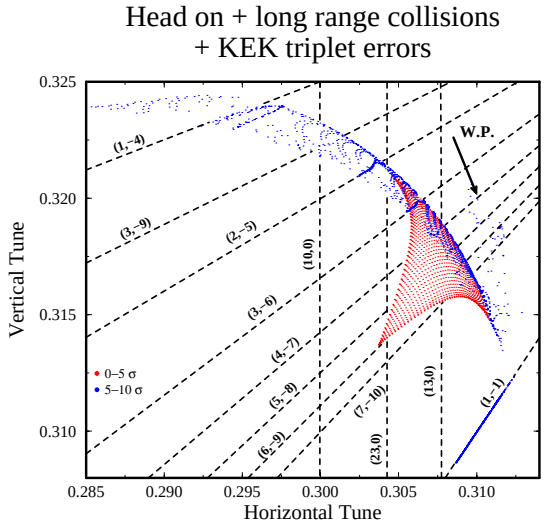

Figure 13: Zimmermann's results for the footprints with the FNAL field errors. Red: $0 \ldots 5\sigma$, blue: $6 \ldots 10\sigma$

out beam-beam collisions, but FNAL or KEK triplet errors, the steep rise happens above 8σ.

Fig. 17 shows the action diffusion rate as a function of the half crossing angle for given initial amplitudes $5\sigma_{x,y}$. A steep rise of the diffusion rate happens below ± 150 μr half crossing angle which corresponds to about $9.5\sigma'_{x,y}$.

Fig. 18 shows the action diffusion rate as a function of the amplitude function β^* at the interaction points for given initial amplitudes $5\sigma_{x,y}$. The half crossing angle is varied at the same time such that it remains at $9.5\sigma'_{x,y}$. A steep rise of the diffusion rate happens below $\beta^* \approx 0.35$ m.

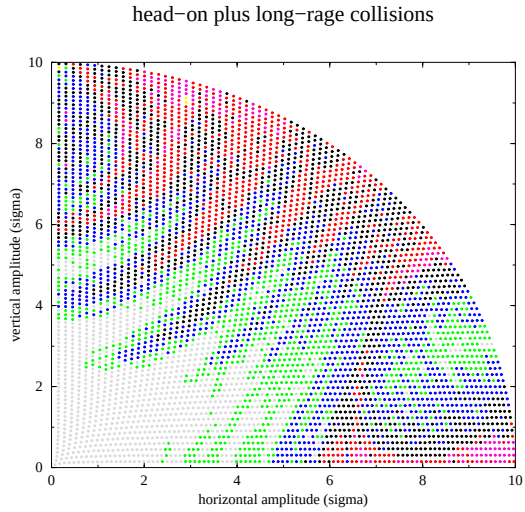

Figure 14: Zimmermann's results for the tune diffusion rate without field errors. Grey $\log \Delta Q \leq -7$; green $-7 \leq \log \Delta Q \leq -6$; blue $-6 \leq \log \Delta Q \leq -5$; black $-5 \leq \log \Delta Q \leq -4$; red $-4 \leq \log \Delta Q \leq -3$; magenta $-3 \leq \log \Delta Q \leq -2$; yellow $-2 \leq \log \Delta Q \leq -1$

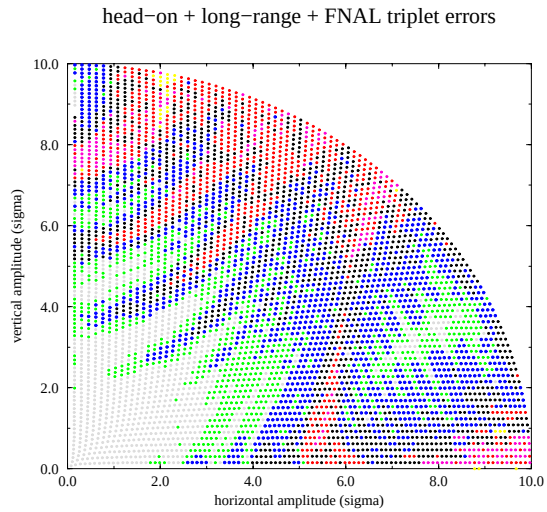

Figure 15: Zimmermann's results for the tune diffusion rate with the FNAL field errors; colour code as in Fig. 14.

8 QUESTIONS FOR THE WORKING GROUP ON WEAK-STRONG EFFECTS

This chapter contains our answers to the remaining question for the working group on weak-strong beam-beam effects.

Can we give a recommendation for the minimum beam separation?

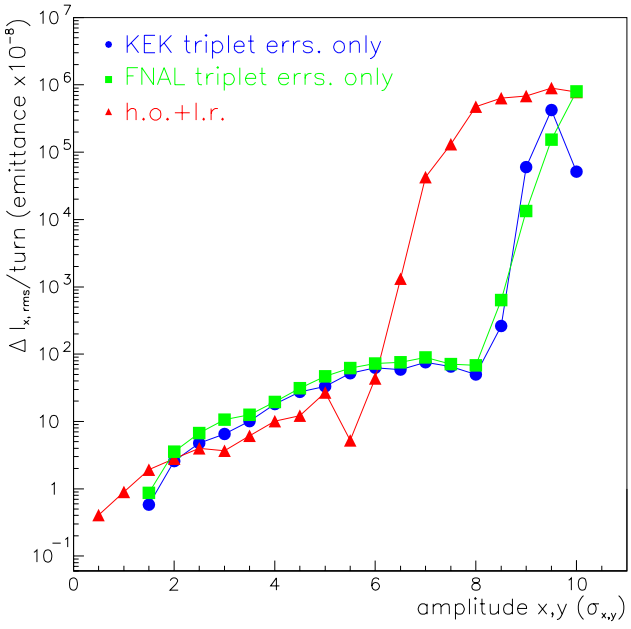

Figure 16: Zimmermann's results for the action diffusion rate vs. initial amplitude for various beam-beam configurations and triplet errors

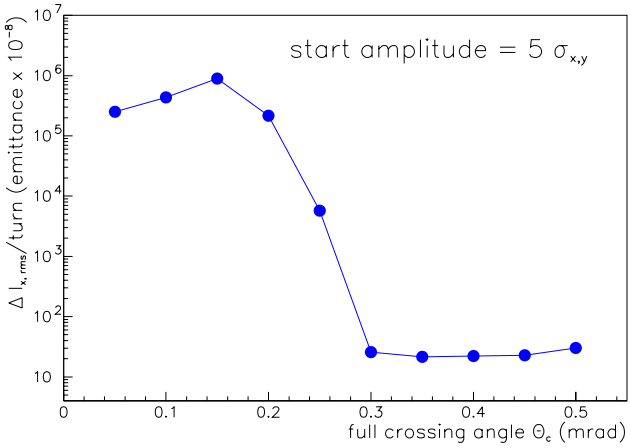

Figure 17: Zimmermann's results for the action diffusion rate vs. full crossing angle at initial amplitudes $5\sigma_{x,y}$

The answer is implied in the discussion of the crossing angle in the previous chapter.

How can we measure and control the head-on collision of the bunches?
By measuring luminosity bunch by bunch, beam-beam luminosity scans, and beam-beam deflection scans. The collision point moves along beam while scanning in the plane of crossing, and luminosity monitors must cover this range. Beam-beam luminosity scans done only at end of fills in the Tevatron, and rarely done in HERA when $\xi \leq 0.002$. Continuous beam-beam scans for the LHC at an amplitude $\sigma/10$ were discussed at another workshop that took place

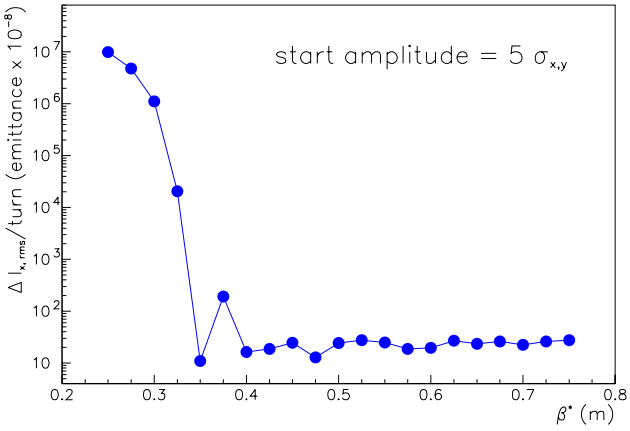

Figure 18: Zimmermann's results for the action diffusion rate vs. β^* at initial amplitudes $5\sigma_{x,y}$

at CERN at the same time as the LHC Beam-Beam Workshop.

Are missing head-on collisions harmful?
We hope not. Fig. 4 demonstrates that the distortion of the footprint by a missing head-on collision is small. We raised the question whether a bad batch can be dumped and refilled individually, or whether all batches must be dumped and refilled.

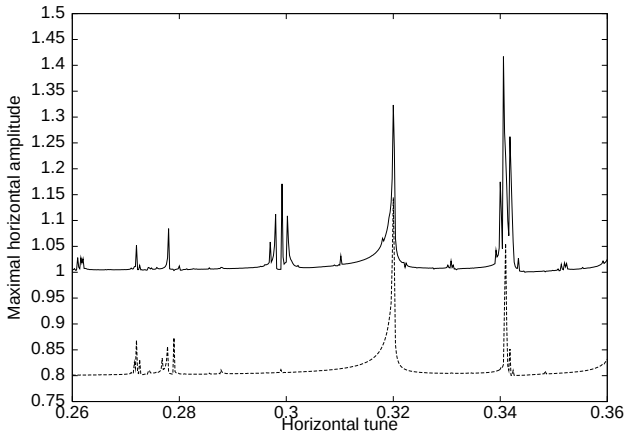

Figure 19: Maximum relative horizontal amplitude due to synchro-betatron resonances with ± 100 μr crossing angle (full line) and without (dashed line). The latter is shifted down by 0.2 units. The horizontal tune is $63.26 \leq Q_x \leq 63.36$. The vertical and synchrotron tunes are $Q_y = 59.32$, and $Q_s = 0.00212$

How much dispersion can we expect and tolerate at the crossing points?
Given the crossing angle and a knowledge of closed orbit errors, the expected values of the dispersion D at the interaction points can be computed. L. Leunissen found that $|D| \approx 6$ mm from the separation bumps is smaller than $|D| \approx 25$ mm from closed orbit errors after correction.

The tolerable D can be found from the analogy with the crossing angle Θ for synchro-betatron resonance excitation $D_y = \alpha C\Theta/4\pi Q_s \approx 100$ mm. The question was raised whether one can correct D and orbit around LHC simultaneously, as is now done in LEP. The side effects of D compensation by either launching forced D oscillation through the arcs or by coupling D_x into D_y by skew quadrupoles in the arcs are unknown.

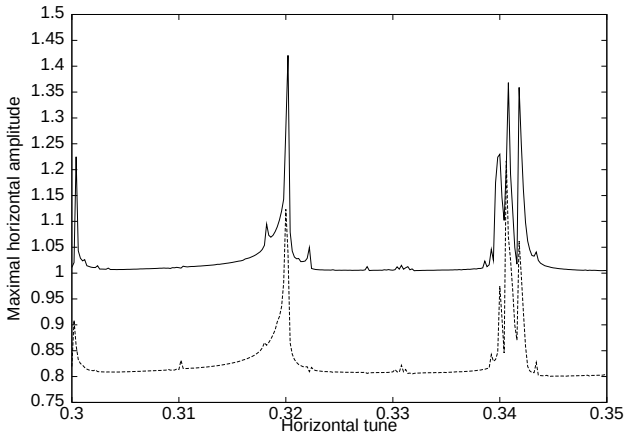

Figure 20: Maximum relative horizontal amplitude due to synchro-betatron resonances with ± 100 μr crossing angle and vertical dispersion $D_y = 0.1$ m (full line) and $D_y = 0$ (dashed line). The latter is shifted down by 0.2 units. The horizontal tune is $63.26 \leq Q_x \leq 63.36$. The vertical and synchrotron tunes are $Q_y = 59.32$, and $Q_s = 0.00212$

Figs. 19 to 21 show results that L. Leunissen obtained with the beam-beam simulation code BBC[5]. Tab. 1 shows his standard assumptions. Fig. 19 shows the maximum relative amplitude reached in a horizontal tune scan. Without crossing angle, the resonances $q_x = q_y$ and $4q_x + 2q_y = 2$ are excited. Here q denotes the fractional part of the tune Q. With crossing angle, the resonance $4q_x + 2q_y = 2$ gets sidebands, and the resonance $10q_x = 3$ is excited and gets sidebands. Fig. 20 shows the maximum relative amplitude reached in another horizontal tune scan. With crossing angle, but without vertical dispersion, the full line in Fig. 19 is reproduced. When vertical dispersion is added, the sidebands of the resonances $q_x = q_y$ and $4q_x + 2q_y = 2$ are more pronounced. Fig. 21 demonstrates that adding $D_y = 0.1$ m to the half crossing angle ± 100 μr causes a few percent extra loss in luminosity.

9 CONCLUSIONS

Simulations by H. Grote, T. Sen and F. Zimmermann agree that the parasitic collisions cause a lower limit on the crossing angle at about ± 150 μr. Sen's results in Fig. 7 yield a maximum of the dynamic aperture at ± 150 μr. Grote found by tracking with LHC data similar to those used for Fig. 5, that particles with amplitudes 7σ were lost above $\Phi = 45^\circ$ for $\pm 175\mu$r (and for $\pm 200\mu$r). However, with the fractional

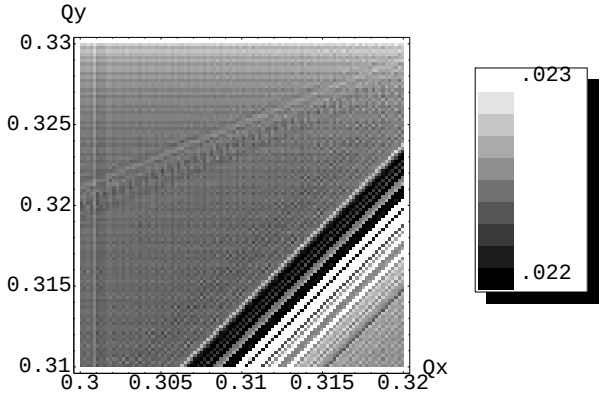

Figure 21: Relative luminosity change between $D_y = 0.1$ m and $D_y = 0$ at ± 100 μr crossing angle

tunes swapped, i.e. $Q_x = 63.32$, $Q_y = 59.31$ the particles survived at $\pm 175\mu$r and were only lost at $\pm 200\mu$r above $\Phi = 45^\circ$. It is advisable to work close to the lower limit of the crossing angle in order to avoid the associated drop in luminosity and large particle amplitudes in the insertion quadrupoles.

The effects of multipole errors in the triplet quadrupoles have become clearer. The results of F. Schmidt demonstrate that they cause a limitation of the dynamic aperture even in the absence of beam-beam collisions, whose value depends on how the FNAL and KEK quadrupoles are installed. T. Sen gave results for the dynamic aperture with triplet errors and with and without beam-beam collisions. Adding the beam-beam collisions reduces the dynamic aperture by 0.7σ within 10^3 turns, and by about 3σ within 10^5 or 10^6 turns. F. Zimmermann demonstrated that higher tune diffusion rates occur at lower particle amplitudes when the triplet errors are added to the beam-beam effects. He also showed that the action diffusion rate quickly increases above 6σ when head-on and long-range beam-beam collisions are added to the triplet errors. With triplet errors alone, the increase in the action diffusion rate happens above 8σ.

Progress in simulation codes hopefully continues, but much remains to be done. There are no comparisons between two programs that use exactly the same machine descriptions, including all the errors. There is no agreed upon way of presenting the results. There is no single program that people in several places use with confidence, contrary to the situation for lattice programs.

The LHC Beam-Beam Workshop was an opportunity for interacting with colleagues whom one sees only too rarely. I should like to thank all participants in the Working Group on Weak-Strong Beam-Beam Effects for their contribution.

10 REFERENCES

[1] Chao-A; Johnson-D; Peggs-S; Peterson-J; Saltmarsh-C; Schachinger-L; Meller-R; Siemann-R; Talman-R; Morton-P; Edwards-D; Finley-D; Gerig-R; Gelfand-N; Harrison-M; Johnson-R; Merminga-N; Syphers-M.; Experimental investigation of nonlinear dynamics in the Fermilab Tevatron. Physical-Review-Letters **61** (1988) 2752

[2] Standard eXchange Format SXF on WWW: www.agsrhichome.bnl.gov/LHC/software/

[3] Gourber, J P ; Hereward, H G ; Myers, S. Overlap knock-out resonances in the CERN Intersecting Storage Rings (ISR), IEEE Trans. Nucl. Sci. **24** (1977) 1405-1407

[4] LHC error tables, valid on 20 March 1999, on WWW: www.agsrhichome.bnl.gov/LHC/kek/v2.0/mqxa_col_v2p0.txt www.agsrhichome.bnl.gov/LHC/fnal/v2.0/hgq_col_v2p0.txt

[5] K. Hirata, BBC User's Guide; A Computer Code for Beam-Beam Interaction with a Crossing Angle, version 3.4, SL-Note 97-57 AP (1997)